Optical Engineering

OpticalEngineering.SPIEDigitalLibrary.org

Application of a long-range swept source optical coherence tomography-based scheme for dimensional characterization of multilayer transparent objects

Eneas N. Morel
Nélida A. Russo
Jorge R. Torga
Ricardo Duchowicz

SPIE.

Eneas N. Morel, Nélida A. Russo, Jorge R. Torga, Ricardo Duchowicz, "Application of a long-range swept source optical coherence tomography-based scheme for dimensional characterization of multilayer transparent objects," *Opt. Eng.* **56**(8), 084102 (2017), doi: 10.1117/1.OE.56.8.084102.

Application of a long-range swept source optical coherence tomography-based scheme for dimensional characterization of multilayer transparent objects

Eneas N. Morel,[a] Nélida A. Russo,[b,*] Jorge R. Torga,[a] and Ricardo Duchowicz[b,c]
[a]Universidad Tecnológica Nacional, Facultad Regional Delta, Laboratorio de Optoelectrónica y Metrología Aplicada, Campana, Buenos Aires, Argentina
[b]Centro de Investigaciones Ópticas (Consejo Nacional de Investigaciones Científicas y Técnicas, Comisión de Investigaciones Científicas de la Provincia de Buenos Aires, Universidad Nacional de La Plata), Gonnet, La Plata, Buenos Aires, Argentina
[c]Universidad Nacional de la Plata, Facultad de Ingeniería, La Plata, Buenos Aires, Argentina

Abstract. This work presents the use of a recently developed interferometric system based on the swept source optical coherence tomography (SS-OCT) technique, which allows the characterization of transparent and semitransparent multilayer systems employing a tunable fiber-optic laser with a coherence length suitable for achieving long-deep range imaging (>10 cm). The inclusion of fiber Bragg gratings in the system allows it to perform a self-calibration in each sweep of the light source. Measurements carried out on cuvettes, ampoules, small bottles, and glass containers used in the pharmaceutical industry are presented. The thicknesses of the walls and the distance between them were determined. Transparent and semitransparent objects of a multilayer type of different thicknesses were also measured. The configuration presented allows extension of the measurement range obtainable with the usual OCT systems, demonstrating the potentiality of the proposed scheme to carry out quality control in industrial applications. [DOI: 10.1117/1.OE.56.8.084102]

Keywords: optical coherence tomography; optical metrology; nondestructive testing; interferometry; laser applications.

Paper 170855 received Jun. 5, 2017; accepted for publication Jul. 18, 2017; published online Aug. 18, 2017.

1 Introduction

Optical coherence tomography (OCT)[1] is a noninvasive interferometric technique that provides real-time three-dimensional (3-D) volumetric images with micrometric resolution and depth of penetration that can range from a few millimeters to tens of centimeters, depending on the technique employed and the material under study. OCT images provide structural information of a sample, based on backscattered light from different layers of material within it. This technique is considered the optical analogue to ultrasound; however, it achieves a higher resolution using near-infrared wavelengths, at the cost of decreasing depth of penetration. Its main application area is medicine, especially ophthalmology and cardiology, where commercial equipment of significant features has been developed and relevant studies have been performed. For example, its use was proposed for blood glucose monitoring, which was tested *in vivo* and *in vitro*. It was shown that OCT is capable of detecting changes in blood glucose concentration as small as a clinically acceptable value of 20 mg/dl.[2,3] On the other hand, Mariampillai et al. reported imaging of microcirculation by calculating the "speckle" variance of OCT from structural images acquired using a Fourier domain mode-locked swept-wavelength laser. They showed that the technique can visualize vessel-size-dependent vascular shutdown and transient vascular occlusion during photodynamic therapy.[4]

Low-coherence interferometric techniques such as OCT have increased their use in industrial metrological applications such as the measurement of very thin thicknesses in semiconductor wafers,[5,6] surface characterization,[7,8] thickness control of the coating of tablets in the pharmaceutical industry,[9] etc. OCT systems based on fiber optics are particularly suitable for use in industrial,[10] hostile (electromagnetic interference, radioactive, cryogenic, or very high temperatures),[11] or difficult-to-access[12] environments.

However, applications such as 3-D inspection in large parts (greater than a centimeter) constitute a little explored area, since its implementation still has some technological limitations.[13]

The SS-OCT technique offers an interesting alternative using tunable light sources that have evolved considerably in recent years,[14] obtaining remarkable sweeping speeds. Among the most interesting are fiber-optic lasers tunable by Fabry–Perot filters of variable spacing or electro-optical modulators, and semiconductor lasers tunable by intracavity refractive index change or the use of MEMS cavities.[15,16] In general, in these systems, it is possible to achieve a narrower emission linewidth and, as a consequence, allow the measurement of distances greater than the centimeter, which considerably broadens the range of applications.[17] In addition, with a high speed of data acquisition and submicrometric resolution, the OCT technique is adaptable to perform both online and offline measurements.[18,19]

In this context, this work shows the application of a recently implemented system,[20] based on the optical fiber technology and SS-OCT technique, for the dimensional characterization of transparent and semitransparent objects of industrial interest with dimensions up to several centimeters,

*Address all correspondence to: Nélida A. Russo, E-mail: nelidar@ciop.unlp.edu.ar

0091-3286/2017/$25.00 © 2017 SPIE

which can also be adapted to perform profilometry of opaque objects. In particular, it is intended to demonstrate that the proposed system is suitable for measuring relevant dimensions in glass containers used in the beverage and pharmaceutical industries. Results obtained from the measurement of the internal and external diameters as well as of the wall thickness of these types of containers are presented. Next, measurements on samples consisting of several glass–air interfaces are displayed to show the system's ability to evaluate dimensions in more complex elements such as conduction systems, refrigeration, or heat exchangers, etc. that exhibit this type of structure. An additional characteristic of the system is its self-calibration capability. This is based on the use of a set of fiber Bragg gratings (FBGs), which let us relate the spatial frequency and the time for each sweep of the light source.

2 Measurement Scheme

The measurement system is based on a Michelson interferometer as shown in Fig. 1, which produces a frequency modulated interference signal generated by the coherent superposition of the reference and sample beams.

As we discussed in a previous work,[20] the interference signal reaching the photodetector, in a simple situation in which the sample has only one reflective surface, can be expressed as

$$I(k) = I_r S\left(\frac{k-k_0}{\Delta k}\right)\left[1+\frac{I_s}{I_r}+2\sqrt{\frac{I_s}{I_r}}\cos\left(n_g\ \Delta z\ \mathrm{k}\right)\right], \qquad (1)$$

where I_r and I_s are the amplitudes of the reference and sample intensities, respectively, $S(k)$ is the emission spectrum of the light source, k is the wavenumber, $k_0 = 2\pi/\lambda_0$ corresponding to the central wavelength (λ_0) of the source spectrum, and Δk is its spectral width. $n_g\ \Delta z$ is the optical path difference (OPD) (with n_g being the group refractive index of the medium in which light is propagated and Δz being the difference in length between both interferometer arms[1,21–23]). For the applications of interest in this work, this is the variable to be determined. If it is desired to carry out a topographic scanning of the sample, it will be necessary to incorporate a beam scanning system.

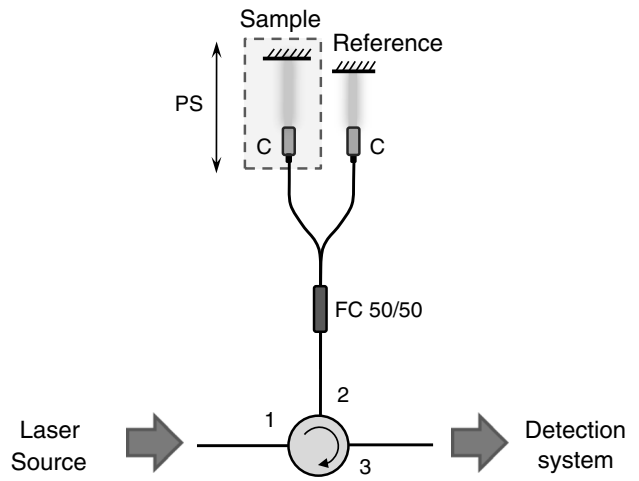

Fig. 1 General scheme (PS, positioning system, C, collimator, FC, fiber coupler).

The Fourier transform of the interference signal obtained for a full spectral scan of the source enables the determination of the OPD between reflecting surfaces. The measurement depth, i.e., the maximum distance that the system can measure ($\Delta z_{\max}$) is determined by Eq. (2), where δ_λ is the spectral resolution of the detection system, $\Delta\lambda$ is the spectral width (in wavelength) of the light source, and N_s is the number of samples[21–23]

$$\Delta z_{\max} = \frac{\lambda_0^2}{4 n_g \delta_\lambda}, \qquad \delta_\lambda = \frac{\Delta\lambda}{N_s}. \qquad (2)$$

The light source was an erbium-doped fiber laser, tunable in the range of 1520 to 1570 nm using a variable-spaced Fabry–Perot filter, which is controlled by a module that allows scanning in the mentioned range.[24] By varying the parameters of the periodic signal applied to the piezoelectric that controls the filter cavity, it is possible to modify the tuning range of the fiber laser and consequently the value of $\Delta z_{\max}$. In addition, considering a rectangular spectral profile when the source is tuned in the above range, the maximum theoretical axial resolution of the measurement system can reach 21 μm, which is derived from the following expression:[1,20]

$$\mathrm{Res} = \frac{2\ \ln(2)}{\pi}\frac{\lambda_0^2}{\Delta\lambda}. \qquad (3)$$

As is well known, FBGs[25] are devices that reflect light within a narrow spectral range centered at the Bragg wavelength for which they were designed. When they are illuminated by a broadband source (or in our case by a swept laser source), they act as filters that block or attenuate light at the Bragg wavelength. Therefore, we use a passive self-calibration system consisting of a set of FBGs centered on different wavelengths within the emission spectrum of the light source. It is intended to obtain attenuation peaks in the interferometric signals that act as marks that relate the emission wavelength of the light source and the temporary position in each sweep. This allows linearizing of the interference spectral signal in the k-space and obtaining the sampling frequency used in the calculation of the Fourier transform. Details on how this was done were discussed in a previously published paper.[20]

3 Experimental Results

The setup implemented for this work corresponds to a single arm Michelson interferometer as shown in Fig. 2. In this type of configuration, the interference signal is generated by the superposition of the reflections in each interface existing in the sample and is able to eliminate errors due to vibrations in the reference arm and a better use of the light source.

To calibrate the system, a set of six fiber Bragg gratings were used. They were centered on the following arbitrarily selected wavelengths: 1529.744, 1539.305, 1539.819, 1544.056, 1547.125, and 1548.991 nm, with spectral widths of 0.1 nm. The aim is to use gratings centered at different known wavelengths, more or less uniformly distributed within the source emission spectrum, although this is not necessary. By associating the temporal positions of the FBGs with the corresponding values of k, a linear relationship was obtained, with a slope of 764.1×10^3 ms^{-1}, resulting in a sampling frequency $f_s = 6543$ m as was explained in Ref. 20.

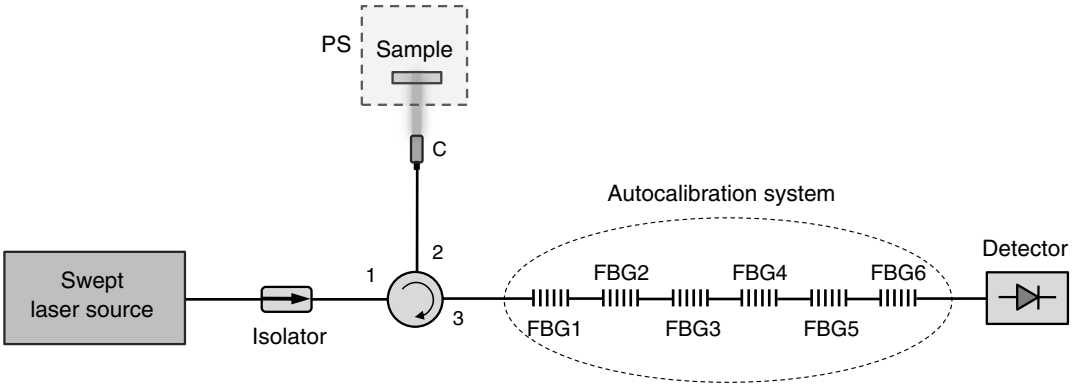

Fig. 2 Implemented measurement system.

The system was used to measure different transparent and semitransparent containers of different sizes, colors, and shapes, as well as to dimensionally characterize multilayer transparent objects to expand the possible applications of the system. The first group of measurements was made on round glass containers (e.g., ampoules and jars used in the pharmaceutical industry, and glass bottles used in the beverage industry), seeking to determine the wall thickness, the internal and external diameters, and the shape in each one. To carry out these measurements, the samples were mounted on a rotating platform that allows measurements to be taken in different sectors. This type of measurement can be used to carry out quality control in the manufacture of such containers. Figure 3 shows, in a generic way, the beams reflected in the different interfaces that appear in the containers as well as the magnitudes involved in the measurement.

Beams reflected in each interface generate the interference signal that will give information about the parameters under study. As is well known, the number of terms in the interference signal is given by the combinatorial number $C_{n,2} = \frac{n!}{2!(n-2)!}$, where n is the number of interfaces. In particular, in this case, six terms are expected to be in the interference signal. An example of the detected intensity is shown in Fig. 4. The attenuation peaks corresponding to the FBGs used to calibrate the measurement are also observed. This temporal distribution was obtained employing a Teledyne LeCroy WaveRunner 610Zi digital oscilloscope and an InGaAs photodetector with 2-GHz bandwidth.

As can be seen in Fig. 5, the Fourier transform of this signal shows "peaks" that correspond to the interference between reflections coming from the boundaries of each material layer (e.g., interference between I_1 and I_2 shown in Fig. 3) and to the interference between reflections at interfaces corresponding to different layers (e.g., interference between I_1 and I_3 shown in Fig. 3).[1,26]

For that case, considering a container with walls of glass and air inside ($n_1 = n_3 = n_g$ and $n_2 = 1$), the expressions in the k-space and in the transformed space (distances) would be

$$\begin{aligned} I(k) = {} & I_1 + I_2 + 2\sqrt{I_1 I_2}\cos[k(n_g d_1)] \\ & + I_1 + I_3 + 2\sqrt{I_1 I_3}\cos[k(n_g d_1 + d_2)] \\ & + I_1 + I_4 + 2\sqrt{I_1 I_4}\cos[k(n_g d_1 + d_2 + n_g d_3)] \\ & + I_2 + I_3 + 2\sqrt{I_2 I_3}\cos[k(d_2)] \\ & + I_2 + I_4 + 2\sqrt{I_2 I_4}\cos[k(d_2 + n_g d_3)] \\ & + I_3 + I_4 + 2\sqrt{I_3 I_4}\cos[k(n_g d_3)], \end{aligned} \tag{4}$$

and

$$\begin{aligned} I(x) \approx {} & \delta(x) + \delta[x \pm (n_g d_1)] + \delta[x \pm (n_g d_1 + d_2)] \\ & + \delta[x \pm (n_g d_1 + d_2 + n_g d_3)] + \delta[x \pm (d_2)] \\ & + \delta[x \pm (d_2 + n_g d_3)] + \delta[x \pm (n_g d_3)]. \end{aligned} \tag{5}$$

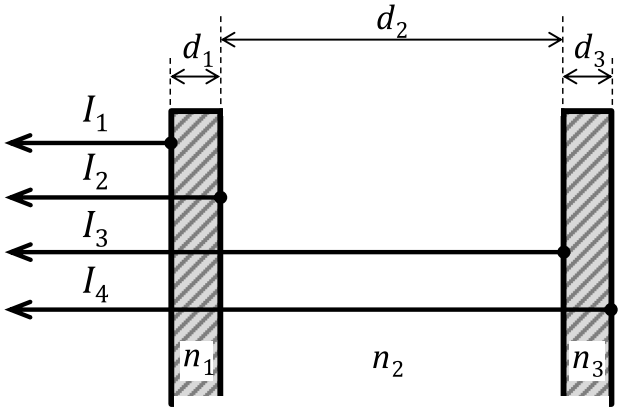

Fig. 3 Beams reflected at different interfaces and dimensions obtained when measuring a jar or container.

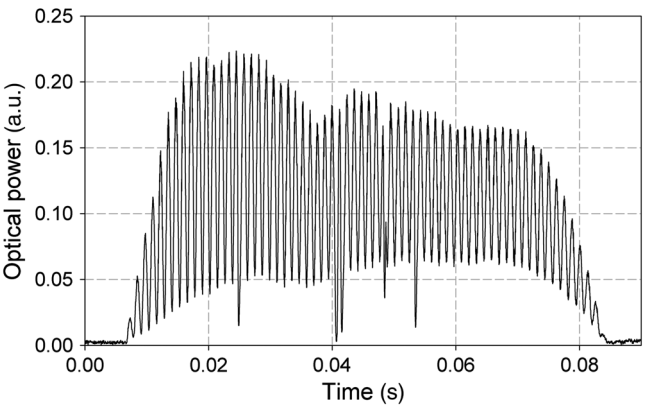

Fig. 4 Typical interferometric signal detected when measuring a jar or container.

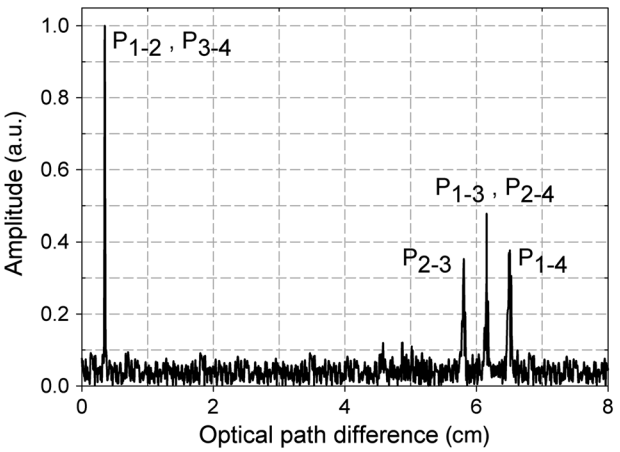

Fig. 5 Fourier transform of the interference signal generated by measuring a glass jar.

We call P_{m-n} to the position (on the OPD axis) of the peak corresponding to the term of the interference signal generated by the reflections I_m and I_n. In general, if n_i is the refractive index of layer (i) of thickness d_i, the position of the interference peaks in the Fourier transform P_{m-n} can be expressed as

$$I_m, I_n \rightarrow P_{m-n} = \sum_{k=m}^{n-1} d_k n_k. \tag{6}$$

Again, considering that the refractive indexes n_1 and n_3 correspond to that of glass and n_2 to that of air, we have

$$I_1, I_4 \rightarrow P_{1-4} = d_1 n_g + d_2 + d_3 n_g. \tag{7}$$

The peak P_{1-2} is superimposed with P_{3-4}, indicating that the thickness of the walls are similar ($d_1 = d_3$). Peak P_{2-3} comes from interference between the beams reflected on the inner walls of the jar. Peak P_{1-3} coincident with P_{2-4} results from the interference between the beams reflected on one of the inner walls and the outer opposing one. Finally, the peak P_{1-4} corresponds to the interference of the beams reflected on the outer walls of the container, resulting in a value of the outer size or external diameter (d_T).

From Eq. (6), we can express the parameters of interest for this case as

$$d_1 = \frac{P_{1,2}}{n_g}, \tag{8}$$

$$d_2 = P_{2,3}, \tag{9}$$

$$d_3 = \frac{P_{3,4}}{n_g}, \tag{10}$$

$$d_T = \frac{P_{1,2} + P_{3,4}}{n_g} + P_{2,3}. \tag{11}$$

If the thicknesses d_1 and d_3 were slightly different, this would be evident by the change in the width of the detected interference peak (this would be wider).[1] As was previously mentioned, the axial resolution of the system is 21 μm; therefore, it will not be able to discern differences in thicknesses smaller than this value.

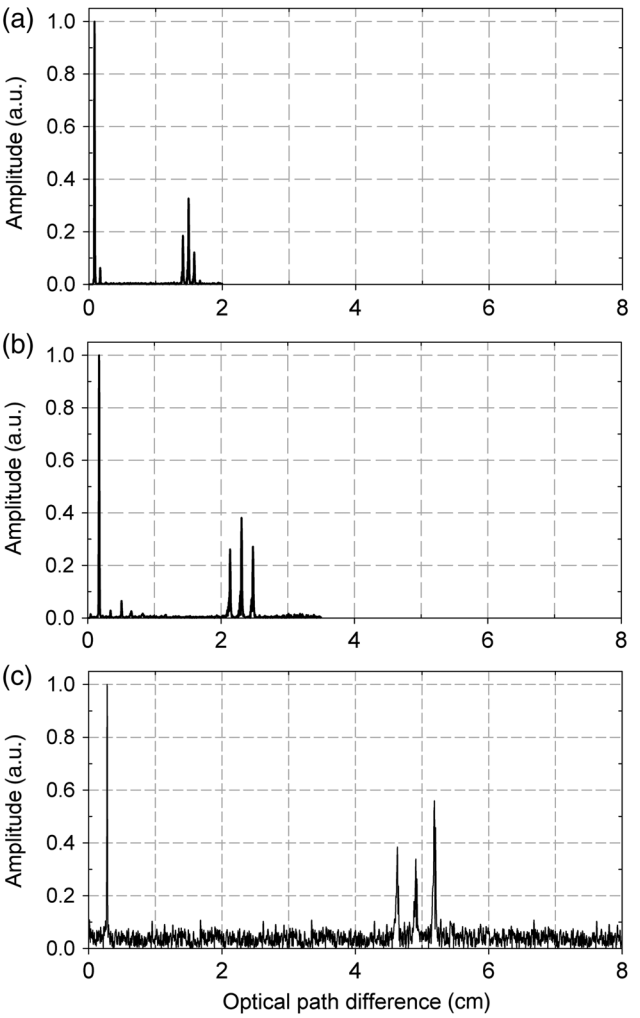

Fig. 6 Fourier transforms of the interference signals obtained by measuring: (a) a glass ampoule, (b) a small glass bottle, and (c) a beaker.

Figure 6 shows the result of processing the detected signals by measuring different transparent objects: (a) a glass ampoule, (b) a small glass bottle, and (c) a beaker. The obtained dimensions are shown in Table 1, whereas Fig. 7 shows a photograph of the experimental setup with one of the samples.

As discussed in Ref. 20, the error in the measurement is determined by the autocalibration process and the bandwidth of the light source, in this case, 50 nm. This gives a peak width in the Fourier transform of the interference signal in the order of 21 μm. With this criterion, we estimate the error in all the measurements at a value of ± 10.5 μm.

From the results obtained, it was decided to extend the measurement possibilities using an experimental scheme that allows a scan over different sectors of the sample. In the arrangement shown in Fig. 7, a platform was used to make a circular scan by rotating the sample around its axis of symmetry. Once the object was moved to the desired measurement position, the resulting interferometric signal data were acquired. Then, the sample was turned to the next measurement position, and the procedure was repeated. In this way,

Table 1 Dimensions obtained when measuring different glass samples.

Sample	d_1, d_3 (cm)	d_2 (cm)	d_T (cm)
(A) Glass ampoule	0.0566	1.41	1.52
(B) Glass bottle	0.12	2.13	2.36
(C) Beaker	0.19	4.62	5.00

the object was momentarily stopped when the data were acquired to carry out the measurement. Figure 8 shows the results obtained when measuring sample (B), and Table 2 summarizes the values obtained after a complete rotation, with measurements angularly spaced every 45 deg.

A second group of measurements was intended to determine the thicknesses corresponding to different multilayer systems, formed by glass plates separated by layers of air of different thicknesses. This type of measurement would allow, for example, the determination of the thickness of internal partitions in containers, helping to carry out quality control during the manufacturing processes. The first sample analyzed consisted of three glass walls and two layers of air, arranged as shown in Fig. 9.

In this configuration, six reflections are generated at the interfaces ($I_j/j = 1, \ldots, 6$). A maximum of 15 peaks is expected when processing the detected optical signal. Glass walls ($G_j/j = 1, 2, 3$) have approximate thicknesses of 0.4 cm (G_1 and G_3) and 0.2 cm (G_2), whereas air zones (A_1 and A_2) have thicknesses of around 0.045 cm.

Figure 10(a) shows a simulation performed with the values corresponding to each of the thicknesses measured with a gauge, which allows identification of the peaks of interference that should appear. Those higher amplitude peaks indicate that there is more than one interface with the same thickness. Figure 10(b) shows the experimental result obtained when measuring the same multilayer object with the proposed optical measurement system. There, the same number of interference peaks located in the same spatial positions is observed, so it is evident that this system is capable of characterizing large multilayer samples. The values of the different thicknesses measured with the SS-OCT system were $A_1 = 0.042$ cm, $A_2 = 0.042$ cm, $G_1 = 0.48$ cm, $G_2 = 0.22$ cm, and $G_3 = 0.48$ cm.

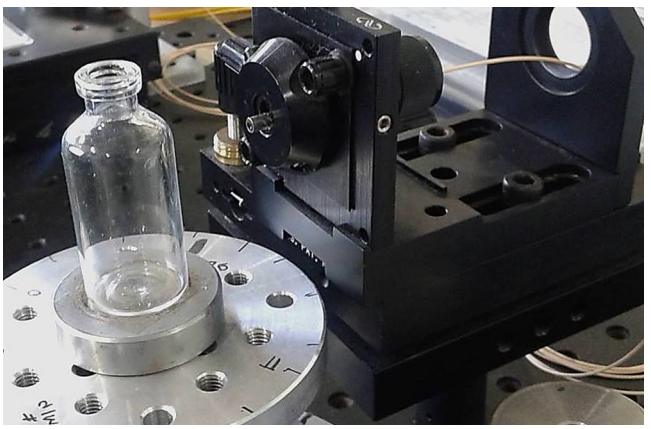

Fig. 7 Glass bottle whose thickness and internal and external diameters are measured at different points on its circumference.

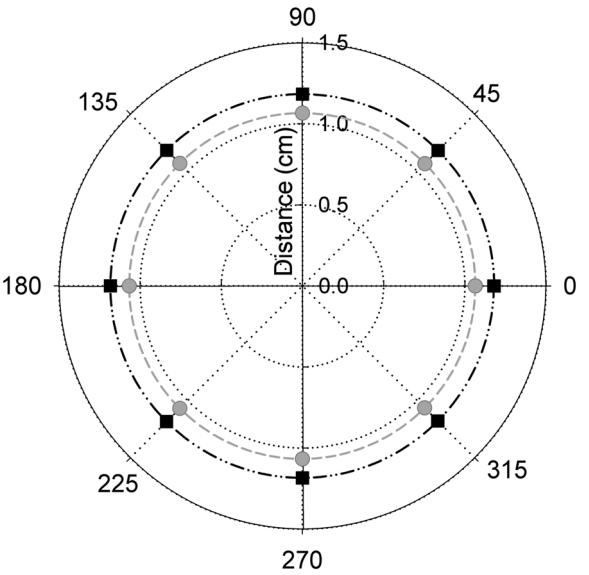

Fig. 8 Measurement of internal (circles) and external (squares) diameters of the sample (B), when rotating on its axis of symmetry.

In Fig. 10(b), only those peaks that provide relevant information to directly determine the searched dimensions were labeled. The extra peaks correspond to the interference of beams reflected on other interfaces (i.e., I_1 and I_3, I_1 and I_5, etc.) and contain information of different combinations between the thicknesses analyzed.

The second multilayer sample analyzed was a system consisting of four glass plates separated by layers of air arranged as shown in Fig. 11. The approximate values of its thicknesses, mechanically determined were $A_1 = 0.37$ cm, $A_2 = 0.36$ cm, $A_3 = 0.37$ cm, $G_1 = 0.48$ cm, $G_2 = 0.10$ cm, $G_3 = 0.10$ cm, and $G_4 = 0.48$ cm.

In this case, there are eight interfaces that generate reflections, which would indicate a maximum number of 28 interference peaks in the Fourier transform of the detected signal.

Table 2 Thickness of the walls (d_1, d_3), internal (d_2), and external diameters (d_T) of sample (B), when measured at different points on its circumference

Angular position (deg)	d_1, d_3 (cm)	d_2 (cm)	d_T (cm)
0	0.1178	2.1273	2.3598
45	0.1146	2.1313	2.3601
90	0.1178	2.1301	2.3644
135	0.1142	2.1352	2.3639
180	0.1179	2.1316	2.3642
225	0.1138	2.1358	2.3656
270	0.1168	2.1334	2.3675
315	0.1143	2.1271	2.3554
360	0.1143	2.1271	2.3554

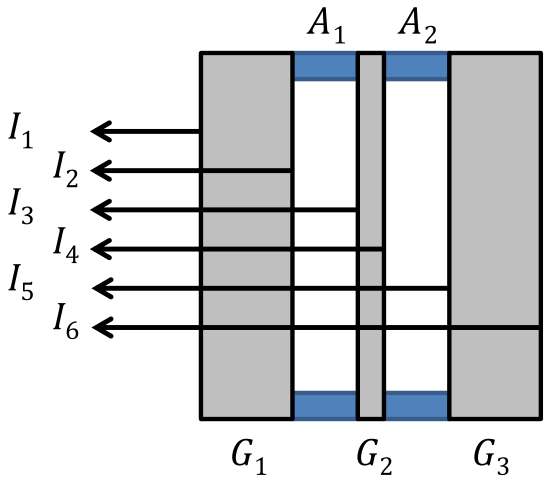

Fig. 9 Multilayer system consisting of three glass partitions separated by two layers of air.

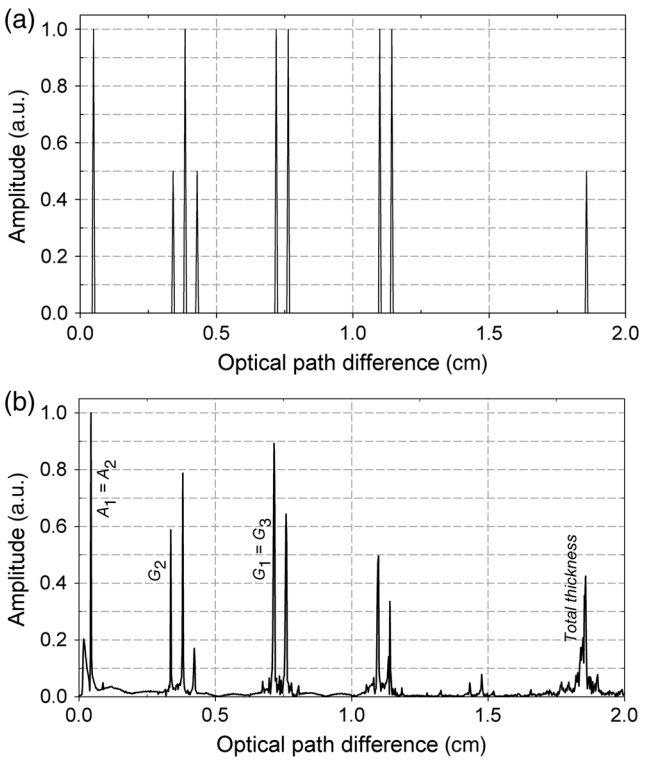

Fig. 10 (a) Simulation of the FFT corresponding to the measurement of a multilayer sample with five thicknesses and (b) experimental result indicating the thicknesses of the sample layers.

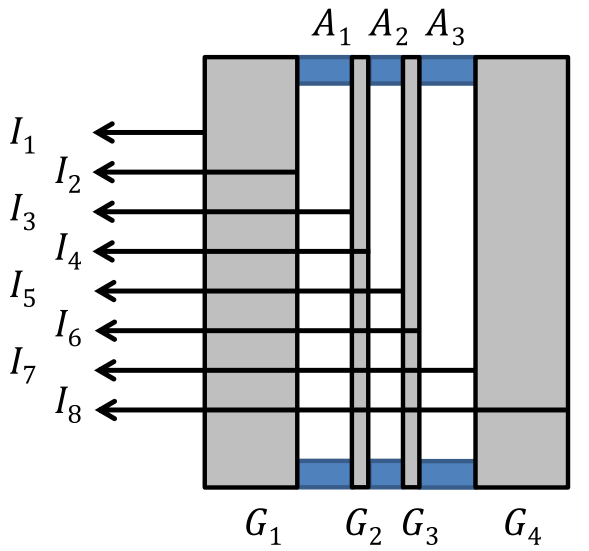

Fig. 11 Multilayer system consisting of four glass partition walls separated by layers of air.

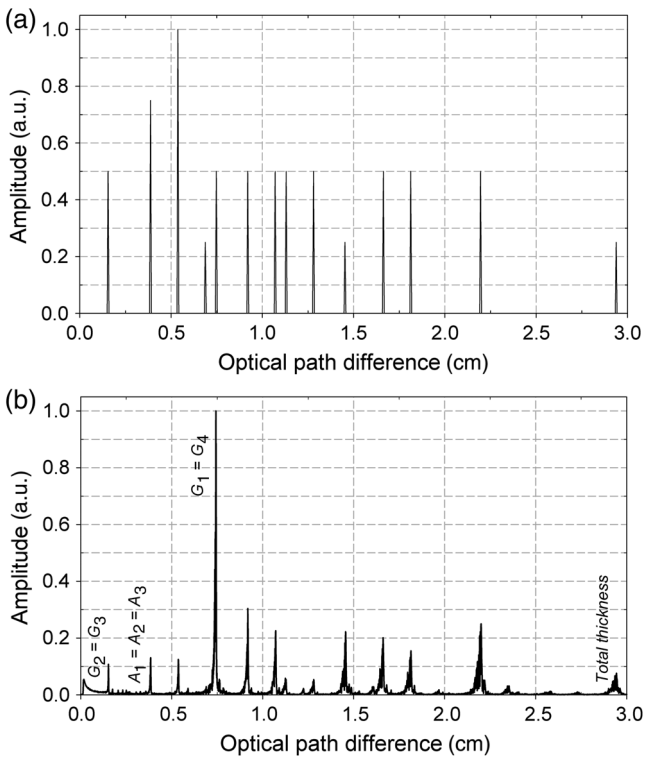

Fig. 12 (a) Simulation of the FFT corresponding to the measurement of a multilayer sample of seven thicknesses and (b) experimental result indicating the different thicknesses of the sample layers.

Undoubtedly, when the number of interfaces begins to increase, it is important to have some prior knowledge of the characteristics of the sample. In this way, it is easier to identify those peaks that provide information of the thicknesses to be measured and to discard those coming from interferences that do not contain relevant information for the dimensional characterization of the sample.

As in the previous case, a simulation of the situation was carried out to determine the amount and position of the interference peaks that were to be expected when processing the detected optical signal. Figure 12(a) shows the 13 interference peaks that must appear due to the characteristics of the sample, since it presents several layers with the same thickness. Figure 12(b) shows the experimental results obtained, which perfectly agree with the simulations performed. The values obtained by the optical measuring system were $A_1 = 0.39$ cm, $A_2 = 0.39$ cm, $A_3 = 0.39$ cm, $G_1 = 0.50$ cm, $G_2 = 0.10$ cm, $G_3 = 0.10$ cm, and $G_4 = 0.50$ cm.

4 Conclusions

The system used was developed to be applied in the characterization of multilayer structures, containers, and glass and

plastic bottles. In this work, it was shown that it is possible to measure wall thicknesses in these types of elements and to make a mapping of the inner and outer diameters in a range greater than 6 cm. The possibility of measuring systems with more than eight interfaces was also shown. In all cases studied for this type of sample, no limitations of the technique have been observed either by the number of peaks that arise in the analysis of the interference signal or by the attenuation produced by the large number of reflections in the different interfaces of the samples.

Using the proposed configuration based on a tunable laser in the region of 1550 nm and a passive self-calibration stage implemented with fiber Bragg gratings, the possibility of measuring a long range of distances was demonstrated. The axial resolution of the system was 21 μm, indicating a minimum value where it is unable to differentiate or detect separately two slightly different thicknesses in a multilayer sample.

These results are very encouraging in the progress toward one of the objectives sought in this work that is to use this technique in the study of multilayer materials used in the packaging industry. Although the measures presented were carried out in a laboratory system, future work will be oriented to the development of systems that can perform online and *in situ* measurements.

Acknowledgments

This work has been funded by the Consejo Nacional de Investigaciones Científicas y Tecnológicas CONICET (No. PIP 112-201101-00397), Facultad de Ingeniería de la Universidad Nacional de la Plata (Proyecto I169), Comisión de Investigaciones Científicas de la Provincia de Buenos Aires CIC (Resolución No. 1266/14), and Facultad Regional Delta, Universidad Tecnológica Nacional (PID 2221), Campana, Argentina.

References

1. D. Huang et al., "Optical coherence tomography," *Science* **254**, 1178–1181 (1991).
2. R. V. Kuranov et al., "Prediction capability of optical coherence tomography for blood glucose concentration monitoring," *J. Diabetes Sci. Technol.* **1**, 470–477 (2007).
3. H. Ullah, F. Hussain, and M. Ikram, "Optical coherence tomography for glucose monitoring in blood," *Appl. Phys. B* **120**, 355–366 (2015).
4. A. Mariampillai et al., "Speckle variance detection of microvasculature using swept-source optical coherence tomography," *Opt. Lett.* **33**, 1530–1532 (2008).
5. W. Walecki et al., "Non-contact fast wafer metrology for ultra-thin patterned wafers mounted on grinding and dicing tapes," in *IEEE/CPMT/SEMI 29th Int. Electronics Manufacturing Technology Symp.*, pp. 323–325 (2004).
6. W. J. Walecki et al., "Low-coherence interferometric absolute distance gauge for study of MEMS structures," *Proc. SPIE* **5716**, 182 (2005).
7. G. Guss et al., "High-resolution 3-D imaging of surface damage sites in fused silica with optical coherence tomography," *Proc. SPIE* **6720**, 67201F (2007).
8. W. J. Walecki et al., "Interferometric metrology for thin and ultra-thin compound semiconductor structures mounted on insulating carriers," in *CS Mantech Conf.* (2004).
9. G. Hannesschläger et al., "A device and a method for monitoring a property of a coating of a solid dosage form during a coating process forming the coating of the solid dosage form," GB application 2513581 (A), EP application 2799842 (A1), US application 020140322429 (A1) (2014).
10. W. J. Walecki and F. Szondy, "Fiber optics low-coherence IR interferometry for defense sensors manufacturing," *Proc. SPIE* **7322**, 73220K (2009).
11. M. L. Dufour et al., "Low-coherence interferometry, an advanced technique for optical metrology in industry," *Insight–Non-Destr. Test. Cond. Monit.* **47**(4), 216–219 (2005).
12. M. Dufour et al., "Inspection of hard-to-reach industrial parts using small diameter probes," *SPIE Newsroom* (2006).
13. S. Song, J. Xu, and R. K. Wang, "Long-range and wide field of view optical coherence tomography for in vivo 3D imaging of large volume object based on a kinetic programmable swept source," *Biomed. Opt. Express* **7**, 4734–4748 (2016).
14. T. Klein and R. Huber, "High-speed OCT light sources and systems," *Biomed. Opt. Express* **8**, 828–859 (2017).
15. M. Bonesi et al., "A-kinetic all-semiconductor programmable swept-source at 1550 nm and 1310 nm with centimeters coherence length," *Opt. Express* **22**, 2632–2655 (2014).
16. R. Huber, M. Wojtkowski, and J. G. Fujimoto, "Fourier domain mode locking (FDML): a new laser operating regime and applications for optical coherence tomography," *Opt. Express* **14**, 3225–3237 (2006).
17. I. Grulkowski et al., "High-precision, high-accuracy ultra long range swept-source optical coherence tomography using vertical cavity surface emitting laser light source," *Opt. Lett.* **38**, 673–675 (2013).
18. W. J. Walecki et al., "High-speed high-accuracy fiber optic low-coherence interferometry for in situ grinding and etching process monitoring," *Proc. SPIE* **6293**, 62930D (2006).
19. ZebraOptical Optoprofiler Probe, http://zebraoptical.com/Interferometric-Probe.html.
20. E. N. Morel et al., "Interferometric system based on swept source optical coherence tomography scheme applied to the measurement of distances of industrial interest," *Opt. Eng.* **55**(1), 014105 (2016).
21. K. Iiyama, L. T. Wang, and K. I. Hayashi, "Linearizing optical frequency sweep of a laser diode for FMCW reflectometry," *J. Lightwave Technol.* **14**, 173–178 (1996).
22. I. Grulkowski et al., "High-precision, high-accuracy ultra long range swept-source optical coherence tomography using vertical cavity surface emitting laser light source," *Opt. Lett.* **38**, 673–675 (2013).
23. C. M. Eigenwillig et al., "K-space linear Fourier domain mode locked laser and applications for optical coherence tomography," *Opt. Express* **16**, 8916–8937 (2008).
24. A. Giordana and R. Duchowicz, "Development and analysis of a simple tunable erbium ring laser," *Proc. SPIE* **8011**, 80115A (2011).
25. R. Kashyap, *Fiber Bragg Gratings*, 2nd ed., Academic Press, Elsevier, Burlington, Massachusetts (2010).
26. H. Ullah et al., "Autocorrelation optical coherence tomography for glucose quantification in blood," *Laser Phys. Lett.* **12**, 125602 (2015).

Eneas N. Morel is an electronic engineer who graduated from the Faculty of Engineering, National University of La Plata (UNLP) in 2003. He received his PhD from the Delta Regional Faculty, National University of Technology, in 2010. He is currently a researcher at the Laboratorio de Optoelectrónica y Metrología Aplicada, Facultad Regional Delta, National University of Technology and a member of Consejo Nacional de Investigaciones Científicas y Técnicas (CONICET), Argentina. His research focuses mainly on low coherence interferometry applied to general metrology and optical coherence tomography applied to the study of materials.

Nélida A. Russo received her MS degree and PhD in engineering from the UNLP, Argentina, in 1985 and 2006, respectively. She is a researcher at the Commission of Scientific Research of Buenos Aires Province (CIC), Argentina. She worked as an assistant professor of physics at the Faculty of Engineering, UNLP. In 1988, she joined the Optical Research Center (CIOp), Argentina, and her current research interests include optical fiber applications in sensors, lasers, and optical communications.

Jorge R. Torga received his degree in physics and his PhD in science from the University of Buenos Aires in 1992 and 1997, respectively. He is currently a researcher at the Laboratorio de Optoelectrónica y Metrología Aplicada, Facultad Regional Delta, National University of Technology and a researcher at CONICET, Argentina. His research focuses mainly in optical coherence tomography and low-coherence interferometry techniques.

Ricardo Duchowicz received his MS degree and PhD in physics from UNLP, in 1981 and 1977, respectively. He is a researcher at the National Council for Scientific and Technical Research (CONICET) and professor at the National University of La Plata (Faculty of Engineering-UNLP), Argentina. In 1977, he joined the CIOp. He has published extensively on subjects related to fiber-optic lasers, fiber sensors, and pulse transmission in fiber-optic links.